Spin-isospin strength distributions for fp shell nuclei: Results for the ^{55}Mn(n,p), ^{56}Fe(n,p), and ^{58}Ni(n,p) reactions at 198 MeV

S. El-Kateb,[1] K.P. Jackson,[2] W.P. Alford,[3] R. Abegg,[2] R.E. Azuma,[4] B.A. Brown,[5] A. Celler,[3] D. Frekers,[2] O. Häusser,[6] R. Helmer,[2] R.S. Henderson,[2,7] K.H. Hicks,[2] R. Jeppesen,[6] J.D. King,[4] K. Raywood,[7] G.G. Shute,[7] B.M. Spicer,[7] A. Trudel,[6] M. Vetterli,[2] and S. Yen[2]

[1] *King Fahd University of Petroleum and Minerals, Dhahran, Saudi Arabia*
[2] *TRIUMF, 4004 Wesbrook Mall, Vancouver, British Columbia, Canada V6T 2A3*
[3] *University of Western Ontario, London, Ontario, Canada N6A 3K7*
[4] *University of Toronto, Toronto, Ontario, Canada N6A 3K7*
[5] *Michigan State University, East Lansing, Michigan 48824*
[6] *Simon Fraser University, Burnaby, British Columbia, Canada V5A 1S6*
[7] *University of Melbourne, Parkville, Victoria 3052, Australia*

(Received 17 February 1994)

Cross sections for the reactions ^{55}Mn(n,p), ^{56}Fe(n,p), and ^{58}Ni(n,p) have been measured at an incident energy of 198 MeV, with protons observed over a range of energies corresponding to excitations of up to about 35 MeV in the residual nuclei ^{55}Cr, ^{56}Mn, and ^{58}Co, respectively. Measurements were carried out at center-of-mass angles between 1.6° and 19.9°. A multipole analysis of the results yielded the distribution of Gamow-Teller (GT) and spin-dipole strength for each target. The total GT strength below an excitation energy of 8.5 MeV was 1.7 units for ^{55}Mn, 2.9 units for ^{56}Fe, and 3.8 units for ^{58}Ni. Shell model calculations of the GT strength distribution, carried out in a restricted vector space, show fair to good agreement with the data up to an excitation energy of 8.5 MeV, but overestimate the total strength by a factor of between 3 and 4.

PACS number(s): 25.40.Kv, 24.30.Cz, 27.40.+z

I. INTRODUCTION

The isovector response of nuclei may be studied using the nucleon charge-exchange reactions (p,n) or (n,p), as well as by a number of other reactions such as $(^3$He,$t)$, $(d,^2$He), or heavy ion reactions. Studies of the energy dependence of the (p,n) reaction [1, 2] have shown that at incident energies of 200 to 300 MeV the spin-flip part of the isovector effective interaction is much stronger than the non-spin-flip part, so that these reactions provide a convenient probe of the spin-isospin response of nuclei, provided the effective interaction is known.

At forward angles and low excitation in the final nucleus, the momentum transfer is small with the result that the reaction cross section is dominated by Gamow-Teller (GT) transitions with $\Delta L = 0$, $\Delta J^\pi = 1^+$. It has been shown that for (p,n) and (n,p) reactions the 0° cross sections for such transitions are proportional to the squares of the matrix element for the GT β decay between the same states [3–5], at least for strong transitions, so that measurements of the reaction cross section can be analyzed to provide a quantitative determination of GT strength distribution in beta decay.

There has been extensive interest in the determination of the distribution of the isospin-raising strength, GT$^+$, for nuclei in the iron-nickel region in connection with the problem of supernova formation [6–8]. In the evolution of a massive star, following depletion of sources of fusion energy in the core, the core becomes unstable to catastrophic collapse. In calculating the onset of collapse and possible supernova formation, an essential ingredient is the electron capture cross section for the nuclei in the mass region around $A = 56$ which make up the stellar core. This cross section is proportional to the GT$^+$ strengths of the core nuclei, which are determined in the present measurements. Bethe *et al.* [6] were the first to appreciate the importance of GT$^+$ strength in this problem, and thus to realize that electron capture might proceed much more rapidly than had been previously estimated. The experimental results are important not only for the direct determination of GT$^+$ strength distributions of stable nuclei, but as a calibration of the model calculations which must be used to estimate strength distributions for unstable nuclei, or for excited states of the target.

Measurements of GT$^+$ strength distributions for several (fp) shell nuclei have been carried out at TRIUMF [9–13] and the present work represents an extension of those earlier results. In addition, measurements of the ^{54,56}Fe (n,p) cross section have been reported at a beam energy of 97 MeV [14]. A related study of the ^{56}Fe$(^{12}$C,^{12}N) reaction at an energy $E/A = 70$ MeV has also been reported [15].

II. EXPERIMENTAL MEASUREMENTS

Measurements were carried out using the TRIUMF charge-exchange facility in the (n,p) mode, which is shown schematically in Fig. 1. In the present measure-

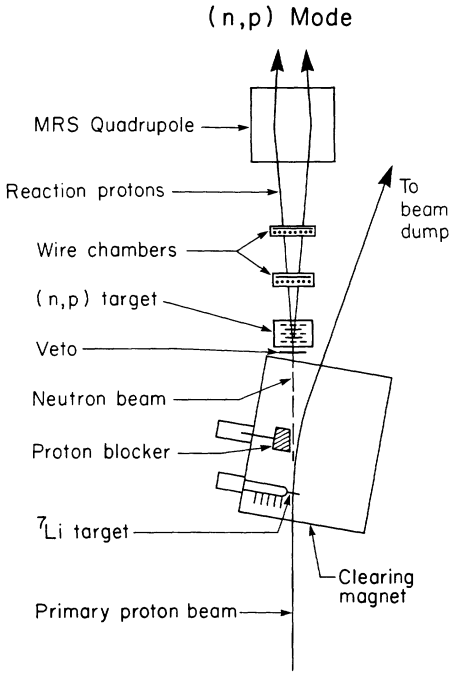

FIG. 1. Schematic layout of the TRIUMF (n,p) facility.

ments the primary proton beam with nominal energy of 200 MeV was incident on a target of ^{7}Li with a thickness of 220 mg/cm^2, producing a secondary neutron beam of energy 198 MeV. With a primary proton beam current of 300–400 nA, the neutron flux on the secondary targets was about 10^5 n/cm^2 sec over the useful target area of 2 cm × 5 cm. Protons from the (n,p) reaction on the secondary targets then passed through two sets of drift chambers which provided a measurement of position and direction for each proton entering the medium resolution spectrometer (MRS). After momentum analysis in the MRS, particles were detected in a series of drift chambers at the exit of the spectrometer. For a given field setting in the MRS, protons were detected over an energy range corresponding to excitation energies up to about 35 MeV in the final nucleus. The energy spread in the neutron beam was about 1 MeV, and overall resolution including the effect of the thickness of the secondary targets was about 1.3 MeV. A more detailed description of the system is given in Refs. [16, 17].

The secondary target consisted of up to six layers of target material, each mounted between wire chamber planes which allowed identification of the target layer in which the detected protons originated. With this system a correction to the measured proton energy for a given target layer can then be made to account for energy loss in subsequent targets. One of the target layers was of polyethylene (CH_2) and protons from the ^{1}H$(n,p)n$ reaction on the hydrogen in this target were used to normalize the reaction cross section from the secondary target of interest. A full description of the target box is given in Ref. [18]. Details of the targets used in these measurements are as follows.

(i) ^{55}Mn—The target material was manganese powder (325 mesh) with chemical purity of 99.3% (Johnson-Matthey Corp). The powder was contained between Mylar foils 6.4 microns in thickness which were glued to metal frames with aperture 2.5 cm × 6 cm. The thicknesses of the five targets used were determined by weighing to be 239, 219, 201, 191, and 126 mg/cm^2. The uniformity of the targets could not be measured directly, but was estimated to be within 10% of the nominal thickness.

(ii) ^{56}Fe—These targets were foils of natural iron, with purity of > 99% (A.D. McKay). In initial measurements, with reduced energy spread in the neutron beam, five targets of thickness 136 mg/cm^2 were used to provide energy resolution of about 0.8 MeV overall. When these measurements showed no evidence of excitation of resolvable, discrete states, the target thickness was increased to 256 mg/cm^2 in order to increase the count rate. The isotopic composition of the natural iron was ^{54}Fe-6%; ^{56}Fe-92%; ^{57}Fe-2%; ^{58}Fe-0.3%. A correction for the ^{54}Fe content of the foils was made as will be described later. The contributions from ^{57}Fe and ^{58}Fe were expected to be less than the statistical uncertainties in the data, and were ignored.

(iii) ^{58}Ni—Four target foils were available, one with thickness 285 mg/cm^2 and area 50 × 110 mm^2 and three with thickness 297 mg/cm^2 and area 25 × 100 mm^2. The isotopic purity was 99.9%.

In addition to the metallic targets, each stack of six targets included a CH_2 target which was used to monitor neutron flux and detector efficiency, and ultimately to determine reaction cross sections for the metallic targets.

The targets were mounted on a wheel which carried two other target stacks. In the present work, one other stack consisted of six CH_2 targets which provided a measurement of relative neutron flux and detector efficiency as a function of target position. The third stack comprised a single CH_2 target plus five empty frames, which was used to monitor background, and to determine inefficiencies in the wire chamber planes of the target box.

The acceptance of the MRS as a function of focal plane position was determined by varying the MRS magnetic field to move the proton groups from the CH_2 target stack along the focal plane. This measurement also provided the energy calibration of the spectrometer which allowed the measurement of excitation energies with an uncertainty of about 100 keV.

Measurements of double-differential cross sections were

TABLE I. Scattering angles in present measurements.

MRS angle	Mean scattering angle (c.m.)		
(lab.)	^{55}Mn	^{56}Fe	^{58}Ni
0	1.6	2.0	1.8
3		3.4	3.5
4	4.2		
6	6.2	6.1	6.3
8	8.2		
10		10.0	10.2
12	12.2		
15		14.9	15.1
16	16.2		
20		19.9	

carried out at angles shown in Table I. The table shows the angle settings of the MRS, along with the mean center-of-mass scattering angle, as determined by the ray tracing with the front end chambers. At each angle setting, the angular acceptance of the MRS included a range of about $\pm 2°$.

III. DATA ANALYSIS AND RESULTS

Data were recorded event-by-event on magnetic tape. During data acquisition, a fraction of the data was analyzed on-line to monitor the progress of the experiment. The final analysis of all data was carried out off-line using the program LISA.

The cross sections of the (n,p) reactions reported in this work were determined from the measurement of counting rates relative to that from the ^{1}H(n,p) peak originating from the CH_2 target in each target stack. The cross section for the latter reaction was calculated from a phase shift analysis of n-p scattering data using the program SAID (SM 90) [19].

A typical raw spectrum for the reaction ^{nat}Fe(n,p) at an MRS angle of 0° is shown in Fig. 2(a). The peak at the left of the spectrum arises from hydrogen in the Mylar foils of the wire chamber planes of the target box, and possibly from hydrogenous material absorbed on surfaces in the target box. The background spectrum was assumed to be satisfactorily represented by the spectrum from the CH_2 target, and was normalized to the hydrogen peak for background subtraction. The spectrum after background subtraction is shown in Fig. 2b, and is seen to be almost unchanged by the subtraction except for the hydrogen peak itself.

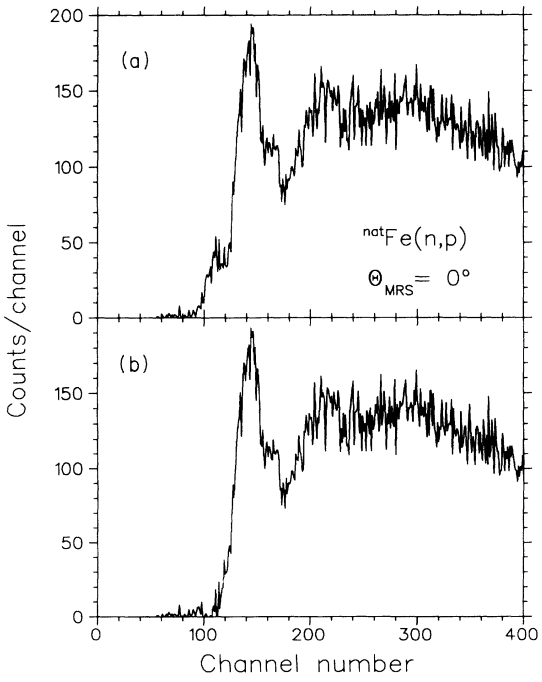

FIG. 2. (a) Raw spectrum for the ^{nat}Fe target measured at MRS angle of 0° (upper panel); (b) spectrum after background subtraction (lower panel).

After background subtraction, spectra were corrected for variation of MRS acceptance with focal plane position, and a deconvolution was carried out to correct for the effect of the weak continuum in the primary neutron spectrum from the ^{7}Li(p,n) reaction. This procedure is described in some detail in Ref. [9]. Finally the data were summed in bins of 1 MeV width to reduce the statistical fluctuations seen in the raw data as in Fig. 2. Final spectra for each target at MRS angles of 0° and 6° are shown in Fig. 3. For each target the 0° spectrum shows a strong peak at low excitation, indicating the presence of GT$^+$ transition strength in this region of excitation.

As noted earlier, the natural iron targets contained about 6% of ^{54}Fe which contributes up to 10% of the measured count rate at low excitation in the 0° spectrum. Data were not available for the ^{54}Fe(n,p) cross section at 198 MeV, but measurements have been reported [9] at 298 MeV. DWIA calculations showed that the magnitude of the peak cross section for $L = 0$ transitions was predicted to change by less than 5% between 300 and 200 MeV. Accordingly, the measured cross section for the ^{54}Fe(n,p) reaction at 0° and 2.5° and 298 MeV was normalized by a factor of 0.06 and subtracted from the present results at 0° and 3°. The resulting spectrum was then renormalized by a factor of 1.06 (=1/0.94) to obtain the final spectrum shown in Fig. 3. Data at 298 MeV were not available at appropriate angles to permit this correction to be made at larger angles, but this lack

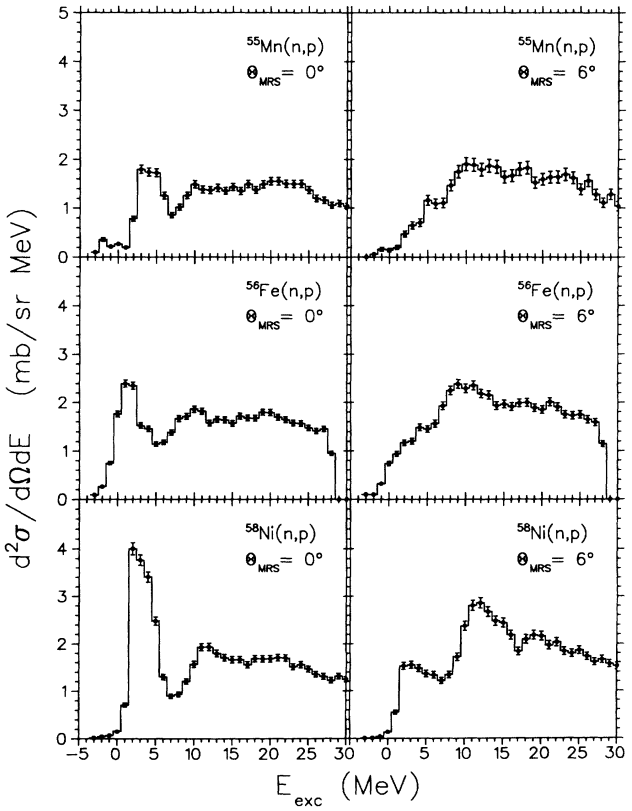

FIG. 3. Final spectra for each target at MRS angles of 0° and 6°. The data have been summed in bins of width 1 MeV.

would not introduce significant uncertainty in the determination of GT^+ transition strength from the data.

As in previous work, the measured spectra were analyzed using a multipole analysis procedure [20] to extract the cross section for GT transitions. In this approach it is assumed that the measured cross section can be represented as an incoherent sum of cross sections for transitions with different spin and parity transfers

$$\frac{d\sigma_{\rm exp}}{dw} = \sum_{\Delta J^\pi} C_{\Delta J^\pi} \sigma_{DW}(\Delta J^\pi) .$$

In principle, the sum should run over all allowed spin and parity transfers consistent with the properties of the initial and final states, with the coefficients $C_{\Delta J^\pi}$ determined by a least-squares fit to the data. In practice, spectra were measured at only five or six angles, so that a maximum of four terms was used in making the analysis of the present results.

For a given orbital angular momentum transfer, ΔL, total angular momentum transfers $\Delta J = \Delta L$, $\Delta L \pm 1$ are possible, with parity change $(-1)^{\Delta L}$. In a previous study [13] of the (n,p) reaction on ^{51}V and ^{59}Co, extensive DWIA calculations were carried out in order to determine the sensitivity of the calculated cross section to the value of ΔJ^π and for a given ΔJ^π, to the particle-hole configuration assumed in the final state. These calculations showed that the shapes of the calculated angular distributions were sensitive mainly to ΔL rather than ΔJ, while for a given ΔL the dependence on the configuration of the final state was small enough that it appeared reasonable to assume that a suitable "average" DWIA shape for each value of ΔL could be obtained by an appropriate choice of the particle-hole configuration.

DWIA cross sections were calculated using the program DW81 [21]. Microscopic optical potentials for incoming and outgoing channels were generated using the code MAINX8 [22], which folded an effective interaction, here the Franey-Love interaction [23], with a matter distribution inferred from electron scattering measurements. The effective interaction used in the impulse approximation calculation was also the Franey-Love interaction. The single particle wave functions describing final configurations were taken as harmonic oscillator functions with a radius parameter $b = 1.9$ fm. These are the same assumptions as were used in the data analysis in Ref. [13]. The particle-hole configurations assumed in the present analysis were also the same as those of Ref. [13], namely, $(\pi\ 0f_{7/2})^{-1}(\nu 0f_{5/2})$ for $\Delta L = 0,2$ and $(\pi\ 0f_{7/2})^{-1}$ $(\nu\ 0g_{9/2})$ for $\Delta L = 1,3$.

For the multipole analysis, DWIA calculations were carried out at 10 MeV intervals, with reaction Q values relative to the ground-state transition spanning the range 5 MeV $\geq$ Q ≥ -35 MeV. The appropriate angular distributions for each energy bin in the data were

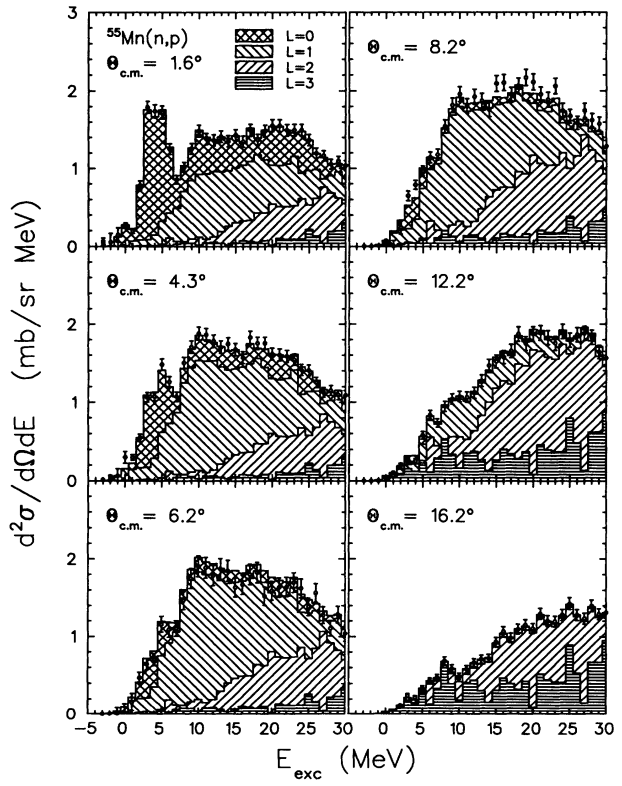

FIG. 4. Results of the multipole decomposition for ^{55}Mn(n,p). At each angle, the contribution of each of the four assumed components is shown. Error bars indicate statistical uncertainties in the fit.

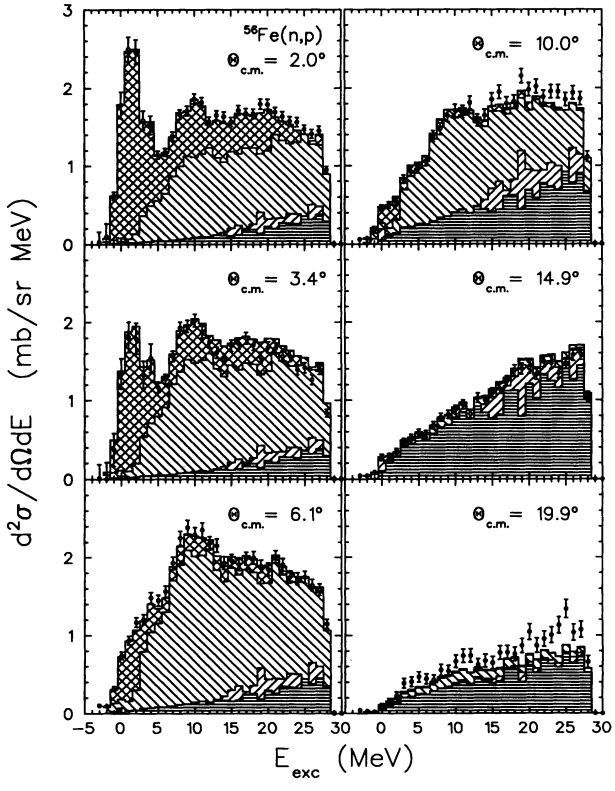

FIG. 5. Results of the multipole decomposition for ^{56}Fe(n,p). At each angle, the contribution of each of the four assumed components is shown. Error bars indicate statistical uncertainties in the fit. The labeling of components is as in Fig. 4.

then obtained by interpolation from these calculations. It should be noted that a fixed particle-hole configuration was assumed for each ΔL over the full range of excitation in the final nucleus, so that the only energy variation in the calculated cross sections arises from kinematic and distortion effects in the DWIA.

The multipole analysis program [20] used the calculated DWIA shapes to make a least-squares fit to the measured angular distribution for each 1 MeV energy bin of the data. The results of this analysis are shown in Fig. 4 for ^{55}Mn(n,p), Fig. 5 for ^{56}Fe(n,p), and Fig. 6 for ^{58}Ni(n,p).

In each case it is seen that there is a strong concentration of $\Delta L = 0$ cross section in the region of the peak in the spectra at the smaller angles. Transitions with ΔL=1 dominate the spectra in the energy range between about 10 to 20 MeV for angles from 4 to 8 degrees. At large angles and high excitation, transitions with ΔL =2 and 3 are dominant. It should be noted that transitions identified as ΔL=3 actually include all transitions with $\Delta L \geq 3$. Also, as in earlier work [13] it was found that the relative contributions for $\Delta L = 2$ and $\Delta L = 3$ are sensitive to the choice of final configuration for $\Delta L = 3$. Thus the total cross section for transitions with $\Delta L > 1$ is well determined in this analysis, but the more detailed decomposition of this cross section is subject to large uncertainties. In this connection, it is interesting to note that the

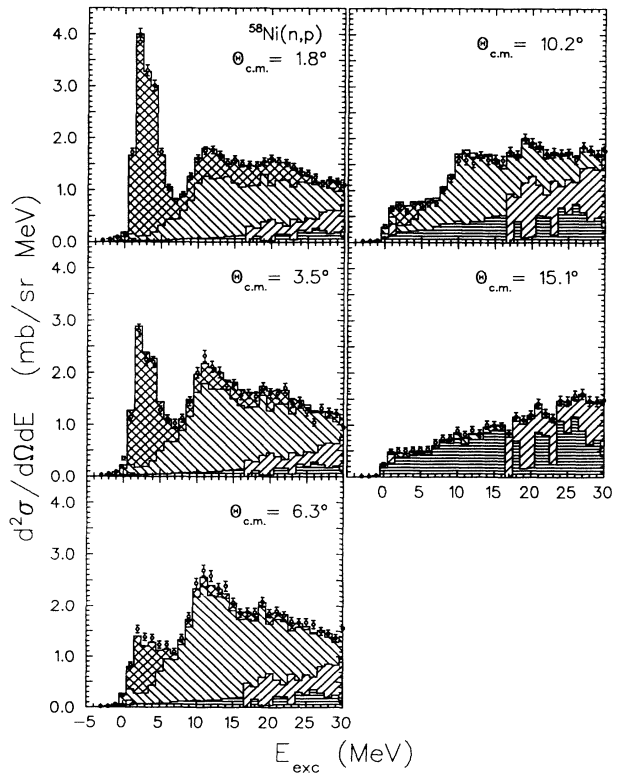

FIG. 6. Results of the multipole decomposition for ^{58}Ni(n,p). At each angle, the contribution of each of the four assumed components is shown. Error bars indicate statistical uncertainties in the fit. The labeling of components is as in Fig. 4.

results of the multipole analysis for ^{55}Mn show that the cross section for the ΔL=2 component is as large as or larger than that for $\Delta L = 3$, while for ^{56}Fe the $\Delta L = 2$ component is much smaller than that for $\Delta L = 3$. It is not clear whether this is a real effect, or whether it reflects the difficulty of separating these components in the multipole analysis.

IV. GAMOW-TELLER STRENGTH

The results of the multipole analyses shown in Figs. 4, 5, and 6 indicate a concentration of transition strength with $\Delta L = 0$ at excitation energies below about 10 MeV, along with a weaker distribution extending over nearly the full range of excitation studied. At low excitation, the measured angular distributions show a clear forward peaking, and the multipole analysis provides a determination of reaction cross section for $\Delta L = 0$ which is very insensitive to the details of the DWIA angular distributions used in the analysis.

At high excitation however, where the reaction cross section is dominated by transitions with $\Delta L > 0$, the measured angular distributions peak at larger angles. In this situation, the estimate of cross section for $\Delta L = 0$ transitions depends sensitively on the detailed shape of the DWIA shape calculated for $\Delta L = 1$ transitions, with the crucial factor being the ratio of 0° cross section to the peak cross section, which occurs at an angle of about 6° for $\Delta L = 1$. This ratio is affected by the choice of the final configuration for the transition, and by the distortions arising from the optical potentials in the incident and exit channels with the result that the estimate of the $\Delta L = 0$ cross section at excitation energies above about 8 MeV is subject to large uncertainties. In spite of these uncertainties, multipole analyses with a variety of plausible model assumptions in the DWIA calculations consistently indicate the presence of some $\Delta L = 0$ cross section at high excitation. It is expected that some GT$^+$ transition strength should be present in this region as a result of the spreading of the $0\hbar\omega$ strength from lower excitation energies [24, 25]. In addition, $2\hbar\omega$ excitations give rise to states of isovector monopole character. DWIA calculations for transitions to these states show a wide variety of angular distribution shapes, often with a marked forward peaking. Thus it is concluded that the measurements identify contributions to the cross section with $\Delta L = 0$ at excitation energies greater than 10 MeV, although the nature of the states involved is not clear. Similar conclusions were reached in an earlier study of the ^{16}O(n,p) reaction at 298 MeV [26].

Gamow-Teller strength distributions have been estimated for each target using the measured cross sections for $\Delta L = 0$ transitions. For each energy bin, the measured cross section at the smallest angle was extrapolated to zero momentum transfer using the DWIA calculations described earlier. The resultant cross sections were then converted to GT$^+$ strength using the ratios $\hat{\sigma} = \sigma(q = 0)/B_{\rm GT}$ obtained by interpolation from measured (p,n) cross sections for transitions between states of known β decay strength [5, 9]. The values of $\hat{\sigma}$ used

in this analysis were 5.00 mb/sr for ^{55}Mn, 4.91 mb/sr for ^{56}Fe, and 4.68 mb/sr for ^{58}Ni. The uncertainties arising from this interpolation are not very well established but are expected to be about 10% [5]. The resulting distributions are shown in Figs. 7, 8, and 9. The total measured strength up to 8.5 MeV excitation was 1.7 ± 0.2 units [where $B(\mathrm{GT}) = 3$ for neutron decay] for ^{55}Mn, 2.9 ± 0.3 units for ^{56}Fe, and 3.8 ± 0.4 units for ^{58}Ni. The quoted uncertainties arise mainly from the estimated 10% uncertainty in $\hat{\sigma}$, plus a smaller statistical uncertainty arising from the multipole analysis.

Shell model calculations for comparison with the measured strength distributions were carried out using the code OXBASH [27]. The calculations were within a truncated vector space as shown in Table II, and used an effective interaction for the *fp* shell which has recently been obtained by Van der Merwe, Richter, and Brown [28] by fitting data for the mass region $41 \geq A \geq 66$. In order to judge the sensitivity of the results to the choice of effective interaction, calculations were also carried out in the same vector space using an effective interaction which has been employed extensively in earlier calculations [29]. The total strengths were nearly equal in the two calculations, and the distribution of strengths with excitation energy were very similar except that the average excitation energy was about 0.7 MeV higher in the second calculation.

In order to model the effect of finite energy resolution in the measurements, the predicted strength of each discrete model state was spread over a Gaussian distribution of width 1.3 MeV corresponding to the experimental energy resolution. The resulting continuous distribution of strength was then summed over bins 1 MeV in width for comparison with the data. In making the comparison, it should be noted that less than 1% of the predicted strength lies at excitation energies above 8.5 MeV. As discussed above and in Ref. [13] the estimate of reaction cross section with $\Delta L = 0$ is subject to large uncertainty at high excitation, and its interpretation in terms of GT$^+$ strength is open to question. As a result, it was concluded that it was reasonable to restrict the model comparison to the region of excitation up to 8.5 MeV. This restriction was also made in Ref. [13], and its use here permits a direct comparison between the present results and those of Ref. [13].

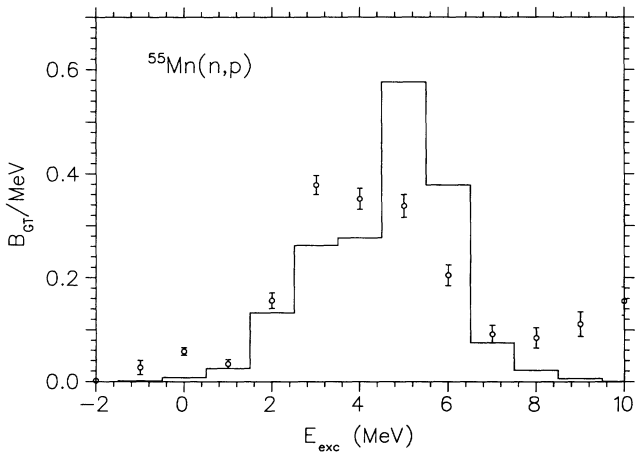

FIG. 7. Comparison of the measured GT$^+$ strength distribution with model predictions for ^{55}Mn. Normalization of the strength corresponds to $B_{\mathrm{GT}} = 3$ for decay of the free neutron. In making this comparison, the calculated strength for each discrete model state was spread over a Gaussian distribution with FWHM = 1.3 MeV, and the resulting continuous distribution was then integrated over bins of width 1 MeV and renormalized as discussed in the text. The result is shown as the histogram.

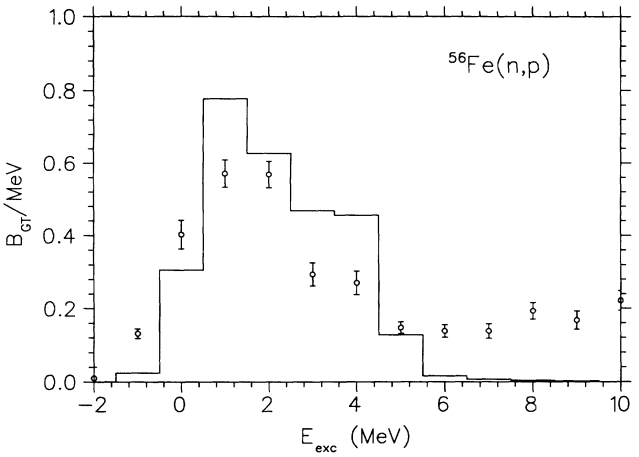

FIG. 8. Comparison of the measured GT$^+$ strength distribution with model predictions for ^{56}Fe. See caption for Fig. 7.

With this restriction, the calculated strength was normalized to the measured strength up to 8.5 MeV. The normalization factors required were 0.23 for ^{55}Mn, 0.31 for ^{56}Fe and 0.31 for ^{58}Ni. These results may be compared directly with the values reported in Ref. [13] 0.23 for ^{51}V and 0.24 for ^{59}Co. In an earlier study of the ^{54}Fe (n,p) reaction at 300 MeV [9], comparison with results of analogous shell model calculations yielded a normalization factor of 0.30 for strength below 10 MeV excitation.

The significance of the normalization factors has been

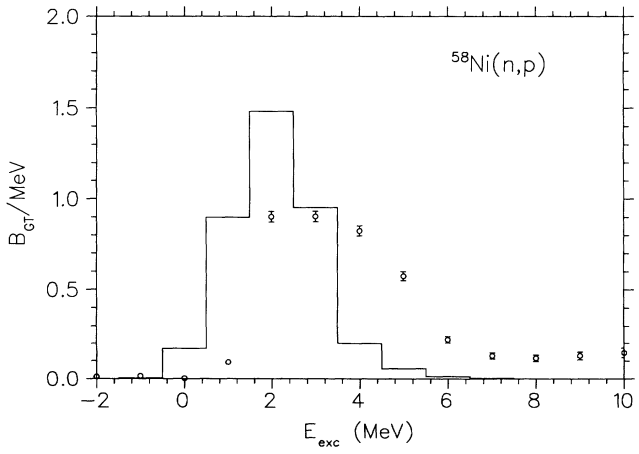

FIG. 9. Comparison of the measured GT$^+$ strength distribution with model predictions for ^{58}Ni. See caption for Fig. 7.

TABLE II. Vector spaces used in shell model calculations.

Target	Parent	Daughter
^{55}Mn	$(f_{7/2})^{13}(f_{5/2}p_{3/2}p_{1/2})^2$	$(f_{7/2})^{12}(f_{5/2}p_{3/2}p_{1/2})^3$
^{56}Fe	$(f_{7/2})^{14}(f_{5/2}p_{3/2}p_{1/2})^2$	$(f_{7/2})^{13}(f_{5/2}p_{3/2}p_{1/2})^3$
^{58}Ni	$(f_{7/2})^{16}(f_{5/2}p_{3/2}p_{1/2})^2$	$(f_{7/2})^{15}(f_{5/2}p_{3/2}p_{1/2})^3$

investigated by Auerbach *et al.* [30] for the GT$^+$ strength in ^{54}Fe and ^{56}Ni. The reduction in strength originates from three contributions (i) the RPA correlations within the fp shell, (ii) higher-order correlations within the fp shell, and (iii) a global reduction by a factor of 0.6 as observed in the sd shell [31] and in (p,n) reactions on heavy nuclei (3). The reduction from the RPA correlations was 0.65 and 0.75 for ^{54}Fe and ^{56}Ni, respectively. The higher-order in-shell correlations are the most difficult to calculate, but the combined effect of the RPA and higher-order correlations was estimated [30] to result in a reduction factor of about 0.62. The combined effect of the in-shell (i) and (ii) and out-of-shell correlations (iii) is thus to give a reduction of about 0.37, which is in qualitative agreement with the values we observed experimentally. But more quantitatively, these results must be nucleus dependent and further calculations are necessary.

The in-shell correlations have been calculated exactly with the Monte Carlo shell-model method [32] and give a reduction factor of 0.37, which is much smaller than the estimate of Auerbach *et al.* However, this result is most sensitive to the $f_{7/2}$-$f_{5/2}$ shell gap, and it will be important to check whether or not the interaction used in [32] gives the observed value for this.

A comparison between the data and the renormalized model calculations is shown in Figs. 7, 8, and 9. In each case, the calculated distribution, shows somewhat sharper peaking than the data, even after broadening to simulate the experimental resolution. For ^{55}Mn and ^{56}Fe, the calculations show reasonable agreement with the data, although the measured strength at low excitation tends to be greater than predicted. For ^{58}Ni however, the model seriously overpredicts the low-lying strength while failing to predict observed strength above 3.5 MeV.

V. ΔL = 1 STRENGTH

The multipole analysis identifies a large contribution to the cross section with $\Delta L = 1$ as shown in Figs. 4, 5, and 6. This is displayed more directly in Fig. 10 which shows the 6° cross section for transitions with $\Delta L = 1$. The resonancelike behavior of the cross sections identifies this as arising mainly from the isovector spin-dipole giant resonance. This resonance contains contributions from transitions with $\Delta J^\pi = 0^-$, 1^-, and 2^-, although the present data do not permit a decomposition into these components. The small $\Delta L = 1$ cross section near zero excitation for each target is probably spurious, and may indicate the uncertainties arising from a multipole analyses for weak transitions. For ^{58}Ni in particular, the lowest known negative parity state in the final nucleus ^{58}Co occurs at 2.8 MeV excitation, so that the peak near zero excitation must be spurious.

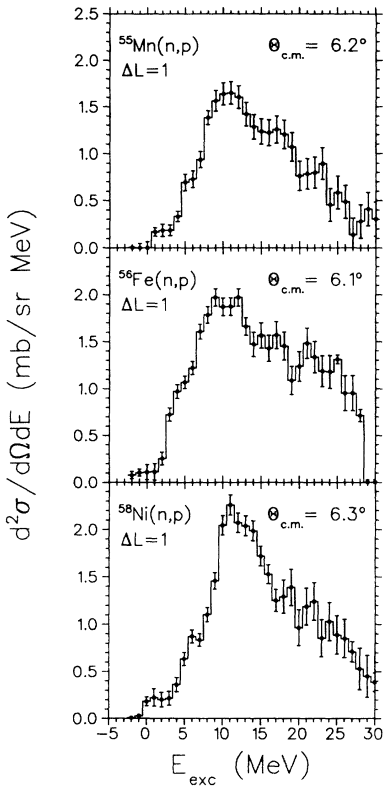

FIG. 10. Energy distributions for $\Delta L = 1$ cross sections at MRS angle of 6°. Error bars represent statistical uncertainties arising from the multipole decomposition.

In spite of this problem, it is believed that the multipole analysis approach provides a realistic estimate of the total cross section for $\Delta L = 1$ transitions. In earlier studies of the ^{51}V, ^{59}Co (n,p) reactions [13] it was found that the estimate of $\Delta L = 1$ cross section was insensitive to the choice of DWIA shapes up to excitation energies of about 20 MeV. At higher energies, the choice of DWIA shape for $\Delta L = 3$ transitions did influence the estimate of $\Delta L = 1$ cross sections although the energy-integrated cross section did not vary by more than about 10% for plausible choices of the particle-hole configuration used in the DWIA calculations.

In the present measurements the energy integrated cross sections up to 30 MeV (28 MeV for ^{56}Fe) at 6° were 25.6 ± 0.8 mb/sr for ^{55}Mn, 36.1 ± 0.8 mb/sr for ^{56}Fe, and 34.8 ± 0.8 mb/sr for ^{58}Ni. The uncertainty quoted represents the statistical uncertainty only resulting from the multipole analysis. The systematic uncertainty arising from the choice of DWIA shapes is estimated to be about 10%.

As seen in Figs. 4, 5, and 6, transitions with $\Delta L > 1$ make important contributions to the cross section at large angles and high excitation energies. The resolu-

tion of this cross section into separate components for different values of ΔL is quite model dependent however, as noted in [13]. The total cross section for these transitions is determined with an uncertainty estimated to be about 25%, but a more detailed decomposition does not appear to be feasible with the present data.

VI. CONCLUSIONS

Measurements of the cross sections for the reactions ^{55}Mn(n,p), ^{56}Fe(n,p), and ^{58}Ni(n,p) have been subjected to a multipole analysis in order to estimate the distributions of GT$^+$ strength from the ground states of these nuclei. These distributions up to an excitation energy of 8.5 MeV have been compared with results of a shell model calculation using a restricted vector space and a new effective interaction. The main features of the data are fitted reasonably well for ^{55}Mn and ^{56}Fe but the centroid of the predicted distribution for ^{58}Ni lies about 2 MeV lower than the measured centroid. The calculated strength is greater than that observed by a factor of about 3 for the even-A targets and a factor of 4 for the odd-A target. These results are consistent with those of earlier measurements of GT$^+$ strength in this mass region Refs. [9–13].

These results provide the data for a useful calibration of model calculations of GT$^+$ strength in this mass region, which should permit more reliable calculations of electron capture rates in the cores of massive stars.

VII. ACKNOWLEDGMENTS

We wish to thank Dr. P.W. Green for help with data acquisition and analysis programs. We also appreciate the assistance of P. Hui and D. Smith in some of the experimental runs. This work was supported by Grants from NSERC Canada, and by NSF Grant No. PHY-90-17077.

[1] T.N. Taddeucci, J. Rapaport, D.E. Bainum, C.D. Goodman, C.C. Foster, C. Gaarde, J. Larsen, C.A. Goulding, D.J. Horen, T. Masterson, and E. Sugarbaker, Phys. Rev. C **25**, 1094 (1981).

[2] W.P. Alford, R.L. Helmer, R. Abegg, A. Celler, O. Häusser, K. Hicks, K.P. Jackson, G.A. Miller, S. Yen, R.E. Azuma, D. Frekers, R.S. Henderson, H. Baer, and C.D. Zafiratos, Phys. Lett. B **179**, 20 (1986).

[3] C.D. Goodman, C.A. Goulding, M.B. Greenfield, J. Rapaport, D.E. Bainum, C.C. Foster, W.G. Love, and F. Petrovich, Phys. Rev. Lett. **44**, 1755 (1980).

[4] K.P. Jackson, A. Celler, W.P. Alford, K. Raywood, R. Abegg, R.E. Azuma, C.K. Campbell, S. El-Kateb, D. Frekers, P.W. Green, O. Häusser, R.L. Helmer, R.S. Henderson, K.H. Hicks, R. Jeppesen, P. Lewis, C.A. Miller, A. Moalem, M.A. Moinester, R.B. Schubank, G.G. Shute, B.M. Spicer, M.C. Vetterli, A.I. Yavin, and S. Yen, Phys. Lett. B **201**, 25 (1988).

[5] T.N. Taddeucci, C.A. Goulding, T.A. Carey, R.C. Byrd, C.D. Goodman, C. Gaarde, J. Larsen, D. Horen, J. Rapaport, and E. Sugarbaker, Nucl. Phys. **A469**, 125 (1987).

[6] H.A. Bethe, G.E. Brown, J. Applegate, and J.M. Lattimer, Nucl. Phys. **A324**, 487 (1979).

[7] G.M. Fuller, W.A. Fowler, and J. Newman, Astrophys. J. **293**, 1 (1985); Astrophys. J. Suppl. **48**, 279 (1982); Astrophys. J. **252**, 715 (1982); Astrophys. J. Suppl. **42**, 477 (1980).

[8] Maurice B. Aufderheide, Stewart D. Bloom, David A. Resler, and Grant J. Mathews, Phys. Rev. C **48**, 1677 (1993).

[9] M.C. Vetterli, O. Häusser, R. Abegg, W.P. Alford, A. Celler, D. Frekers, R. Helmer, R. Henderson, K.H. Hicks, K.P. Jackson, R.G. Jeppesen, C.A. Miller, K. Raywood, and S. Yen, Phys. Rev. C **40**, 559 (1989).

[10] W.P. Alford, R.L. Helmer, R. Abegg, A. Celler, D. Frekers, P. Green, O. Häusser, R. Henderson, K. Hicks, K.P. Jackson, R. Jeppesen, C.A. Miller, A. Trudel, M. Vetterli, S. Yen, H. Pourang, J. Watson, B.A. Brown, and J. Engel, Nucl. Phys. **A514**, 49 (1990).

[11] W.P. Alford, A. Celler, B.A. Brown, R. Abegg, K. Ferguson, R. Helmer, K.P. Jackson, S. Long, K. Raywood, and S. Yen, Nucl. Phys. **A531**, 97 (1991).

[12] M.C. Vetterli, K.P. Jackson, A. Celler, J. Engel, D. Frekers, O. Häusser, R. Helmer, R. Henderson, K.H. Hicks, R.G. Jeppesen, B. Larson, B. Pointon, A. Trudel, and S. Yen, Phys. Rev. C **45**, 997 (1992).

[13] W.P. Alford, B.A. Brown, S. Burzynski, A. Celler, D. Frekers, R. Helmer, R. Henderson, K.P. Jackson, K. Lee, A. Rahav, A. Trudel, and M.C. Vetterli, Phys. Rev. C **48**, 2818 (1993).

[14] T. Rönnqvist, H. Condé, N. Olsson. E. Ramström, R. Zorro, J. Blomgren, A. Håkansson, A. Ringbom, G. Tibell, O. Jonsson, L. Nilsson, P.-U. Renberg, S.Y. van der Werf, W. Unkelbach, and F.P. Brady, Nucl. Phys. **A563**, 225 (1993).

[15] N. Anantaraman, J.S. Winfield, Sam M. Austin, J.A. Carr, C. Djalali, A. Gillibert, W. Mittig, J.A. Nolen, Jr., and Zhan Wen Long, Phys. Rev. C **44**, 398 (1991).

[16] R. Helmer, Can. J. Phys. **65**, 588 (1987).

[17] S. Yen, Can. J. Phys. **65**, 595 (1987).

[18] R.S. Henderson, W.P. Alford, D. Frekers, O. Häusser, R.L. Helmer, K.H. Hicks, K.P. Jackson, C.A. Miller, M.C. Vetterli, and S. Yen, Nucl. Instrum. Methods A **257**, 97 (1987).

[19] R.A. Arndt and L.D. Roper, "Scattering Analysis Interaction Dial-in (SAID) program (SM90)" (unpublished); R.A. Arndt *et al.*, Phys. Rev. D **45**, 3995 (1992).

[20] M.A. Moinester, Can. J. Phys. **65**, 660 (1987).

[21] R. Schaeffer and J. Raynal, Computer Code DWBA70, (unpublished); J.R. Comfort, Computer code DW81 (extended version of DWBA70), Arizona State University, 1984.

[22] T. Cooper, Computer code MAINX8 (private communication); modified by R.G. Jeppesen (unpublished).

[23] M.A. Franey and W.G. Love, Phys. Rev. C **31**, 488

(1985).
[24] G.F. Bertsch and I. Hamamoto, Phys. Rev. C **26**, 1323 (1982).
[25] G.A. Rijsdijk, W.J.W. Geurts, M.G.E. Brand, K. Allaart, and W.H. Dickhoff, Phys. Rev. C **48**, 1752 (1993).
[26] K.H. Hicks, A. Celler, O. Häusser, R. Henderson, K.P. Jackson, B. Pointon, J. Rapaport, M. Vetterli, and S. Yen, Phys. Rev. C **43**, 2554 (1991).
[27] B.A. Brown, A. Etchegoyen, W.D.M. Rae, and N.S. Godwin, The Oxford-Buenos Aires-MSU shell model code (OXBASH), MSUCL Report No. 524, 1986 (unpublished).
[28] M.G. Van der Merwe, W.A. Richter, and B.A. Brown, Nucl. Phys. A (submitted).
[29] W.A. Richter, M.G. Van der Merwe, R.E. Julies, and B.A. Brown, Nucl. Phys. A **523**, 325 (1991).
[30] N. Auerbach, G.F. Bertsch, B.A. Brown, and L. Zhao, Nucl. Phys. A **556**, 190 (1993).
[31] B.A. Brown and B.H. Wildenthal, At. Data Nucl. Data Tables **33**, 247 (1985); Annu. Rev. Nucl. Part. Sci. **38**, 29 (1988).
[32] Y. Alhassid, D.J. Dean, S.E. Koonin, G. Lang, and W.E. Ormand, Phys. Rev. Lett. **72**, 613 (1994).